# Illumination and Spatially Varying Specular Reflectance from a Single View

Kenji Hara
Department of Visual Communication Design
Kyushu University
hara@design.kyushu-u.ac.jp

Ko Nishino
Department of Computer Science
Drexel University
kon@drexel.edu

## Abstract

*Estimating the illumination and the reflectance properties of an object surface from a sparse set of images is an important but inherently ill-posed problem. The problem becomes even harder if we wish to account for the spatial variation of material properties on the surface. In this paper, we derive a novel method for estimating the spatially varying specular reflectance properties, of a surface of known geometry, as well as the illumination distribution from a specular-only image, for instance, captured using polarization to separate reflection components. Unlike previous work, we do not assume the illumination to be a single point light source. We model specular reflection with a spherical statistical distribution and encode the spatial variation with radial basis functions of its parameters. This allows us to formulate the simultaneous estimation of spatially varying specular reflectance and illumination as a sound probabilistic inference problem, in particular, using Csiszár's I-divergence measure. To solve it, we derive an iterative algorithm similar to expectation maximization. We demonstrate the effectiveness of the method on synthetic and real-world scenes.*

## 1. Introduction

Real-world objects and scenes exhibit various appearances resulting from the often tangled interaction of incident illumination, surface geometry, and reflectance properties of the object surfaces. For many applications in computer vision, untangling this complex interaction to sift out some or all of the constituents, namely the illumination, geometry, and reflectance properties, is critical to their success. For instance, estimated illumination can be used to "unshade" the scene, recovered object/scene geometry will provide a direct 3D cue, and inferred reflectance properties can offer unique material classifications, for object/scene recognition and tracking. Such scene information can be directly used for image synthesis applications in computer graphics as well – to achieve photorealistic renderings of the object/scene under novel lighting and from novel viewpoints.

Unfortunately, the problem of recovering illumination, geometry, and reflectance properties from a single image is devastatingly ill-posed. A more realistic and practical problem is to recover as much information as possible from as few images as possible making less assumptions as needed. Past work has tackled this problem from various angles. Among them, many approaches have been proposed to recover the illumination [8], the reflectance properties [15, 2], or both [11] from a large set of images assuming known object geometry. To make the problem tractable, these approaches often assume that the reflectance properties of the object surface are more or less uniform. For instance, Sato et al. [15] assume that the specular reflectance properties of the object surface change very smoothly on the surface such that they can be represented with a small set of sparsely sampled points on the object surface. If we further assume that the specular reflectance properties of the object surface are completely homogeneous across the surface, we may drastically reduce the number of required input images and still simultaneously estimate those parameter values as well as the illumination [6, 13, 14, 9].

Yet, many real-world objects have inhomogeneous reflectance properties across their surfaces. A computational method for estimating both the illumination and reflectance properties of such general object surfaces from a few images would have significant implications for a wide range of applications. Recently, Zickler et al. [19] proposed a framework for recovering spatially varying reflectance properties from a sparse set of images based on the spatial coherence between spatial and angular data. They formulate reflectance estimation as the problem of interpolating scattered data in a mixed spatial and angular domain and stably recovering the spatially varying reflectance by considering the trade-off relation between spatial and angular reflectance resolution. In their work, however, the illumination is assumed to be known in advance. To our knowledge, the problem of recovering spatially varying specular reflectance and scene illumination from a sparse set images

has not been tackled before.

In this paper, we derive a novel method for estimating the spatially varying specular reflectance properties of a surface of known geometry as well as the illumination distribution from a specular-only image – an image that only contains the specular reflection of the surface. Such an image can be captured, for instance, using polarization to separate reflection components. The remaining reflectance property, i.e., the diffuse reflection, can be estimated by unshading the pre-separated diffuse-only image using the estimated illumination, for instance, by assuming Lambertian reflection. Unlike previous methods that achieve the same goal but from a large number of images, we do not assume the illumination to be a single point light source [5].

We make minimal assumptions about the scene illumination and specular reflectance property. We assume that the illumination environment is composed of a set of distant point light sources (directional illumination) and the specular peak corresponding to all sources can be observed in the input specular image. The number and direction of distant point light sources can be estimated by using conventional methods as in [6, 13]. For simplicity, we use a semi-automatic method for achieving this. The light source directions can be easily obtained by calculating the perfect mirror direction at each specular peak pixel and thus the unknown illumination parameters to be estimated are the light source intensities.

We model specular reflection with a spherical statistical distribution and encode the spatial variation with radial basis functions of its parameters. This allows us to formulate the simultaneous estimation of spatially varying specular reflectance and illumination as a variational probabilistic inference problem in which we can canonically devise statistical error measures and derive a robust joint estimation algorithm. In particular, we formulate it as constrained optimization based on Csiszár's $I$-divergence measure [1] and derive an iterative algorithm similar to expectation maximization [3] to solve it. We demonstrate the effectiveness of the method on synthetic and real-world scenes. The results show that we can successfully estimate both the scene illumination and spatially varying specular reflectance properties from a single image and as a result the full reflectance properties may be estimated from only two images from the same view. To our knowledge, this is the first time to demonstrate such capability.

## 2. Spherical Torrance-Sparrow model

The key idea underlying the proposed method is to cast the problem of simultaneously estimating illumination and specular reflectance properties as a probabilistic inference problem so that a joint estimation algorithm based on statistical principals can be derived and devised. For this, the first step is to jointly represent the illumination and the reflectance properties in the same parametric form that enables statistical interpretation. To this end, we consider encoding the specular light interaction with a spherical distribution, i.e., a directional statistics distribution. In particular, we adopt the *spherical Torrance-Sparrow reflection model* recently introduced by Hara et al. [6].

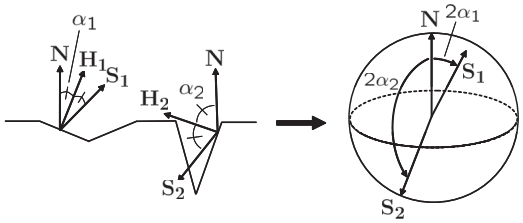


Figure 1. The spherical Torrance-Sparrow reflection model [6] encodes the microfacet orientation distribution of the Torrance-Sparrow reflection model [17] with a directional statistics distribution, namely the von Mises-Fisher distribution [4].

The spherical Torrance-Sparrow reflection model approximates the Torrance-Sparrow reflection model which models specular reflection as the aggregated light reflection from a collection of microfacets lying within a infinitesimally small surface region corresponding to a pixel each having perfect mirror reflection but whose orientations are statistically distributed [17]. Assuming that the distribution of the orientations of microfacets can be modeled with the von Mises-Fisher distribution [4, 10] – a Gaussian distribution on the unit sphere – (see Figure 1), the spherical Torrance-Sparrow reflection model [6] represents specular reflection as

$$\mathbf{I}_S = \int_{-\pi}^{\pi}\int_{0}^{\frac{\pi}{2}} \frac{\mathbf{K}_S F G}{\cos\theta_r} \times L_i(\theta_i,\phi_i)\exp\bigl(-2\kappa\sin^2\alpha\bigr)\sin\theta_i d\theta_i d\phi_i\,, \quad (1)$$

where $\mathbf{I}_S$ denotes a three-band color vector of the specular reflection radiance. As in the original Torrance-Sparrow reflection model, $\mathbf{K}_S$ is the color vector of the specular reflection[1], $F$ is the Fresnel reflectance coefficient, $G$ is the geometrical attenuation factor, $\theta_r$ is the angle between the viewing direction and the surface normal, $\theta_i$ and $\phi_i$ are the polar and azimuth angles, respectively. $L_i(\theta_i,\phi_i)$ is the illumination radiance per unit solid angle coming from the direction $(\theta_i,\phi_i)$, $\sin\theta_i d\theta_i d\phi_i$ is the infinitesimal solid angle, $\alpha$ is the angle between the surface normal and the bisector of the viewing direction and the light source direction [17]. Unique to the spherical Torrance-Sparrow reflection model, $\kappa$ encodes the surface roughness which is related to the surface roughness $\sigma$ of the original Torrance-Sparrow reflection model [17] by $\kappa \simeq 1/4\sigma^2$.

[1]The values of this vector subsumes the normalization factor of the exponential function, the reflectivity of the surface, and the scaling factor between scene radiance and a pixel value

As in the case of the original Torrance-Sparrow reflection model [17], we may simplify Equation (1) by assuming that the Fresnel factor and the geometric attenuation factor remain constant, which is valid for non-grazing angle incident light [16]. Then the specular image irradiance $\mathbf{I}_S(\mathbf{x})$ at image coordinate $\mathbf{x} = (x, y)$ of surface point $P(\mathbf{x})$ can be written as

$$\mathbf{I}_S(\mathbf{x}) = \int_{-\pi}^{\pi}\int_{0}^{\frac{\pi}{2}} \frac{\mathbf{K}_S(\mathbf{x})}{\cos(\theta_r(\mathbf{x}))} \times L_i(\theta_i, \phi_i) \exp\big(-2\kappa(\mathbf{x}) \sin^2 \alpha(\mathbf{x})\big) \sin\theta_i d\theta_i d\phi_i. \quad (2)$$

We assume that the illumination environment can be decomposed into a set of distant point light sources of uniform color $\boldsymbol{L}$, which is valid as long as we have an environmental illumination, e.g., the object size is much smaller compared to the distance to the closest light source, of roughly the same color. Under this assumption Equation (2) can be further reduced and discretized

$$\mathbf{I}_S(\mathbf{x}) \simeq I_S(\mathbf{x})\mathbf{L}, \quad (3)$$

$$I_S(\mathbf{x}) = \frac{2\pi}{N_L} \frac{K_S(\mathbf{x})}{\cos(\theta_r(\mathbf{x}))} \sum_{l=1}^{L} L_l \exp\big(-2\kappa(\mathbf{x}) \sin^2 \alpha_l(\mathbf{x})\big), \quad (4)$$

where all the parameters are scalars: $L_l$ is the magnitude of the color vector of the $l$-th point light source, and $N_L$ is the number of nodes in the geodesic hemisphere [13].

## 3. Probabilistic Formulation

The spherical Torrance-Sparrow reflection model provides a clean directional statistics interpretation of the specular reflection as described in Equation (4), which encodes the interplay of illumination, i.e., the distribution of $L_l$ on a unit hemisphere, and the reflectance parameters $K_s$ and $\kappa$, in a unified representation. We can now formulate the joint estimation of illumination and reflectance properties as simultaneously estimating all parameters in this equation. To proceed, we first rewrite Equation (4) as

$$\widetilde{I}(\mathbf{x}) = \sum_{l=1}^{L} \mathcal{I}_l(\mathbf{x}), \quad (5)$$

$$\mathcal{I}_l(\mathbf{x}) = \widetilde{L}_l K_s(\mathbf{x}) \exp\big(-\kappa(\mathbf{x})\, \omega_l(\mathbf{x})\big), \quad (6)$$

where $\widetilde{I}(\mathbf{x}) = I_S(\mathbf{x}) \cos(\theta_r(\mathbf{x}))$, $\widetilde{L}_l = 2\pi L_l / N_L$, and $\omega_l(\mathbf{x}) = 2\sin^2(\alpha_l(\mathbf{x}))$. Here, we assume that the extrinsic camera parameters are known and thus $\theta_r(\mathbf{x})$ is known. Note, however, that the two unknown parameters $\widetilde{L}_l$ and $K_s(\mathbf{x})$ cannot be uniquely determined from Equation (6): the equation is bilinear in these two parameters. Hence, we impose an additional constraint without loss of generality

$$\sum_{l=1}^{L} \widetilde{L}_l = 1, \quad (7)$$

which corresponds to redefining $\widetilde{L}_l$ as the relative radiance of the $l$-th light source.

In order to represent spatially varying specular reflectance properties, we will assume that the variation of the values of the two parameters $K_s(\mathbf{x})$ and $\kappa(\mathbf{x})$ can be encoded with a set of radial basis functions (RBFs) defined on a uniform grid in the image plane

$$K_s(\mathbf{x}) \simeq K_s(\mathbf{x}; \boldsymbol{\Theta}) \triangleq \exp\Big(\sum_{i=1}^{I} K_i\, \Phi_i(\mathbf{x})\Big), \quad (8)$$

$$\kappa(\mathbf{x}) \simeq \kappa(\mathbf{x}; \boldsymbol{\theta}) \triangleq \sum_{j=1}^{J} \kappa_j\, \phi_j(\mathbf{x}), \quad (9)$$

where the logarithm of the approximating function $K_s(\mathbf{x}; \boldsymbol{\Theta})$ for $K_s(\mathbf{x})$ is represented as a weighted sum of $I$ radial basis functions $\{\Phi_i(\mathbf{x})\}_{i=1}^{I}$ with unknown weight coefficients $\boldsymbol{\Theta} = \{K_i\}_{i=1}^{I}$, while the approximating function $\kappa(\mathbf{x}; \boldsymbol{\theta})$ for $\kappa(\mathbf{x})$ is directly represented as a weighted sum of $J$ radial basis functions $\{\phi_j(\mathbf{x})\}_{j=1}^{J}$ with unknown weight coefficients $\boldsymbol{\theta} = \{\kappa_j\}_{j=1}^{J}$. Also, we use the RBF network for function approximation in the physical parameter space, while most conventional methods directly approximate the observed data (e.g. [19]). Such approaches cannot explain the physical meaning while ours can. Here, we use a Gaussian distribution for each radial basis function

$$\Phi_i(\mathbf{x}) = \exp\Big(-\frac{||\mathbf{x} - \boldsymbol{C}_i||^2}{2R_i^2}\Big) \quad (i = 1, 2, \cdots, I), \quad (10)$$

$$\phi_j(\mathbf{x}) = \exp\Big(-\frac{||\mathbf{x} - \boldsymbol{c}_j||^2}{2r_j^2}\Big) \quad (j = 1, 2, \cdots, J), \quad (11)$$

where $\boldsymbol{C}_i$ and $R_i$ are the center and variance for $\Phi_i(\mathbf{x})$, respectively, and $\boldsymbol{c}_j$ and $r_j$ are the center and variance for $\phi_i(\mathbf{x})$, respectively[2].

By substituting Equations (8) and (9) into Equations (5) and (6), we obtain

$$\widetilde{I}(\mathbf{x}) \simeq \widetilde{I}(\mathbf{x}; \boldsymbol{\Omega}) \triangleq \sum_{l=1}^{L} \mathcal{I}_l(\mathbf{x}; \boldsymbol{\Omega}_l), \quad (12)$$

$$\mathcal{I}_l(\mathbf{x}; \boldsymbol{\Omega}_l) \triangleq \widetilde{L}_l \exp\Big(\sum_{i=1}^{I} K_i\, \Phi_i(\mathbf{x}) - \omega_l(\mathbf{x}) \sum_{j=1}^{J} \kappa_j\, \phi_j(\mathbf{x})\Big)$$

$$= \exp\Big(\ln \widetilde{L}_l + \sum_{i=1}^{I} K_i\, \Phi_i(\mathbf{x}) - \omega_l(\mathbf{x}) \sum_{j=1}^{J} \kappa_j\, \phi_j(\mathbf{x})\Big), \quad (13)$$

where $\boldsymbol{\Omega} = \{\boldsymbol{\Theta}, \boldsymbol{\theta}, \mathcal{L}\} = \{\{K_i\}_{i=1}^{I}, \{\kappa_j\}_{j=1}^{J}, \{\widetilde{L}_l\}_{l=1}^{L}\}$ and $\boldsymbol{\Omega}_l = \{\boldsymbol{\Theta}, \boldsymbol{\theta}, \widetilde{L}_l\} = \{\{K_i\}_{i=1}^{I}, \{\kappa_j\}_{j=1}^{J}, \widetilde{L}_l\}$. The

[2] In this paper, $\{\boldsymbol{C}_i, R_i\}_{i=1}^{I}$, $\{\boldsymbol{c}_j, r_j\}_{j=1}^{J}$, $I$, and $J$ are all assumed to be fixed constants. Estimating these values as variables is a significant problem on its own, which we plan to tackle in the future.

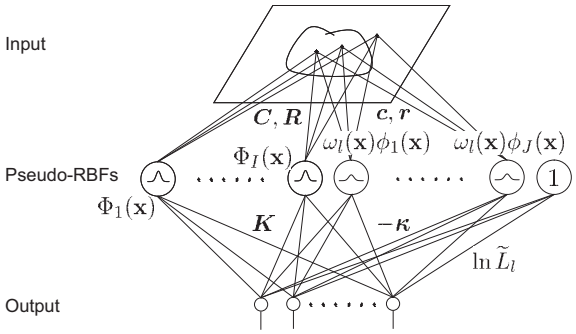


Figure 2. We formulate the joint estimation of spatially varying reflectance and illumination as learning the hidden units of a pseudo-RBF network.

problem of simultaneously estimating the specular reflection parameters $\{K_s(\mathbf{x}), \kappa(\mathbf{x})\}$ and illumination $\mathcal{L} = \{\widetilde{L}_l\}_{l=1}^L$ has thus been formulated as determining the unknown parameters $\mathbf{\Omega} = \{\{K_i\}_{i=1}^I, \{\kappa_j\}_{j=1}^J, \{\widetilde{L}_l\}_{l=1}^L\}$ in Equation (12) and (13). From Equation (13), the joint estimation of the spatially varying reflectance and illumination leads to learning each $l$-th RBF network whose hidden units are $\{\{\Phi_i(\mathbf{x})\}_{i=1}^I, \{\omega_l(\mathbf{x})\phi_j(\mathbf{x})\}_{j=1}^J, 1\}$ and whose second-layer weights are $\{\{K_i\}_{i=1}^I, \{-\kappa_j\}_{j=1}^J, \ln(\widetilde{L}_l)\}$ (Figure 2). Although $\{\omega_l(\mathbf{x})\phi_j(\mathbf{x})\}_{j=1}^J$ are not, strictly speaking, radially symmetric (we refer to them as "pseudo-RBFs"), those functions preserve characteristics of RBF networks such as the locality and the smoothness, and hence convergence and stability properties are preserved.

## 4. Parameter Estimation as Probabilistic Inference

We formulate parameter estimation, $\mathbf{\Omega}$, as a probabilistic inference problem, in which the predicted specular intensities should become as close as possible to the observed intensities. Since we have expressed the predicted values as a directional statistics distribution $\widetilde{I}(\mathbf{x})$, we may naturally measure the discrepancy between this distribution and the observed distribution, which we define as $D(\mathbf{x})$ that encodes the the input specular image irradiance at $\mathbf{x}$ multiplied by $\cos(\theta_r(\mathbf{x}))$, using a statistical measure. In particular, we use Csiszár's $I$-divergence [1] (hereinafter referred to as the "$I$-divergence"), which is a generalization of the well known Kullback-Leibler divergence and is a natural discrepancy measure for nonnegative data,

$$E(\mathbf{\Omega}) = \iint_S \Big( D(\mathbf{x}) \log \frac{D(\mathbf{x})}{\widetilde{I}(\mathbf{x}\,;\mathbf{\Omega})} - \big(D(\mathbf{x}) - \widetilde{I}(\mathbf{x}\,;\mathbf{\Omega})\big)\Big) d\mathbf{x}\,, \quad (14)$$

where $S$ is the image region corresponding to the target surface area. The goal is then to minimize this $I$-divergence with respect to $\mathbf{\Omega} = \{\{K_i\}_{i=1}^I, \{\kappa_j\}_{j=1}^J, \{\widetilde{L}_l\}_{l=1}^L\}$ subject to the constraint given by Equation (7).

The advantage of this statistical formulation is that we can devise sound probabilistic inference algorithms to solve the otherwise tangled joint estimation problem. In other words, we can leverage established alternating minimization algorithms that do not just empirically iterate between minimizing the error function with respect to each parameter set but are constructed based upon the principals of expectation maximization with sound probabilistic interpretations. The problem is well-studied in the signal processing and machine learning communities. Recently, Kameoka et al. [7] derived an iterative algorithm, which is formally similar to expectation maximization, to minimize the $I$-divergence. In this section, we adapt the fundamentals of their optimization technique to derive an iterative algorithm for minimizing the I-divergence in Equation (14).

First, let us introduce a set of functions, $\boldsymbol{m} = \{m_l(\mathbf{x})\}_{l=1}^L$, that satisfies both $m_l(\mathbf{x}) \in (0,1)$ and $\sum_{l=1}^L m_l(\mathbf{x}) = 1$ for $\forall l \in \{1, 2, \cdots, L\}$ and $\forall \mathbf{x} \in S$, and partitions the values of $D(\mathbf{x})$ into $L$ light sources. We refer to these functions as the masking functions. Using these functions, we obtain a useful inequality

$$\begin{aligned} E(\mathbf{\Omega}) \leq & \iint_S \Big( \sum_{l=1}^L m_l(\mathbf{x}) D(\mathbf{x}) \log \frac{m_l(\mathbf{x}) D(\mathbf{x})}{\mathcal{I}_l(\mathbf{x}\,;\mathbf{\Omega}_l)} \\ & \qquad - \sum_{l=1}^L \big( m_l(\mathbf{x}) D(\mathbf{x}) - \mathcal{I}_l(\mathbf{x}\,;\mathbf{\Omega}_l) \big) \Big) d\mathbf{x} \\ = & \sum_{l=1}^L \iint_S \Big( \mathcal{D}_l(\mathbf{x}) \log \frac{\mathcal{D}_l(\mathbf{x})}{\mathcal{I}_l(\mathbf{x}\,;\mathbf{\Omega}_l)} \\ & \qquad - \big( \mathcal{D}_l(\mathbf{x}) - \mathcal{I}_l(\mathbf{x}\,;\mathbf{\Omega}_l) \big) \Big) d\mathbf{x} \triangleq E^+(\mathbf{\Omega}, \boldsymbol{m}), \quad (15) \end{aligned}$$

where $\mathcal{D}_l(\mathbf{x}) = m_l(\mathbf{x}) D(\mathbf{x})$ $(l = 1, 2, \cdots, L)$.

We may then first minimize $E^+(\mathbf{\Omega}, \boldsymbol{m})$ with respect to $\boldsymbol{m}(\mathbf{x})$ while keeping $\mathbf{\Omega}$ fixed, which leads to $E(\mathbf{\Omega}) = E^+(\mathbf{\Omega}, \boldsymbol{m})$ while preserving the inequality in Equation (15). The masking functions $\boldsymbol{m}(\mathbf{x})$ that minimize $E^+(\mathbf{\Omega}, \boldsymbol{m})$ can be obtained analytically as

$$m_l(\mathbf{x}) = \frac{\mathcal{I}_l(\mathbf{x}\,;\mathbf{\Omega}_l)}{\sum_{l=1}^L \mathcal{I}_l(\mathbf{x}\,;\mathbf{\Omega}_l)} \qquad (l = 1, 2, \cdots, L)\,. \quad (16)$$

Then we may minimize $E^+(\mathbf{\Omega}, \boldsymbol{m})$ with respect to $\mathbf{\Omega}$ while keeping $\boldsymbol{m}$ fixed. These two computations are iterated until convergence. This iterative algorithm can be summarized as follows:

**Algorithm**

**Step 1.** Initialize : $\mathbf{\Omega}^{(0)} = \{\{K_i^{(0)}\}_{i=1}^I, \{\kappa_j^{(0)}\}_{j=1}^J, \{\widetilde{L}_l^{(0)}\}_{l=1}^L\}$ , $t \Leftarrow 0$

**Step 2.** Repeat the steps below until *convergence*

$$\textbf{E-step: } \boldsymbol{m}^{(t+1)} \Leftarrow \underset{\boldsymbol{m}}{\operatorname{argmin}}\, E^{+}(\boldsymbol{\Omega}^{(t)}, \boldsymbol{m})$$
$$\textbf{M-step: } \boldsymbol{\Omega}^{(t+1)} \Leftarrow \underset{\boldsymbol{\Omega}}{\operatorname{argmin}}\, E^{+}(\boldsymbol{\Omega}, \boldsymbol{m}^{(t+1)}),$$
$$t \Leftarrow t+1$$

**Step 3.** Output : $K_s(\mathbf{x}) \Leftarrow \exp\big(\sum_{i=1}^{I} K_i^{(t)} \Phi_i(\mathbf{x})\big)$, $\kappa(\mathbf{x}) \Leftarrow \sum_{j=1}^{J} \kappa_j^{(t)} \phi_j(\mathbf{x})$, $\{\widetilde{L}_l\}_{l=1}^{L} \Leftarrow \{\widetilde{L}_l^{(t)}\}_{l=1}^{L}$

---

We will now derive the update equations for $\boldsymbol{\Omega}$ required in **Step 2**. First, the partial derivatives of $E^{+}(\boldsymbol{\Theta}, \boldsymbol{m})$ (Equation (15)) with respect to an $I$-dimensional vector $\boldsymbol{K} = (K_1, \cdots, K_I)^T$ and a $J$-dimensional vector $\boldsymbol{\kappa} = (\kappa_1, \cdots, \kappa_J)^T$ are

$$\frac{\partial E^{+}}{\partial \boldsymbol{K}} = -\sum_{l=1}^{L} \iint_S \big(\mathcal{D}_l(\mathbf{x}) - \mathcal{I}_l(\mathbf{x}; \boldsymbol{\Omega}_l)\big) \boldsymbol{\Phi}(\mathbf{x}) d\mathbf{x}, \quad (17)$$

$$\frac{\partial E^{+}}{\partial \boldsymbol{\kappa}} = \sum_{l=1}^{L} \iint_S \big(\mathcal{D}_l(\mathbf{x}) - \mathcal{I}_l(\mathbf{x}; \boldsymbol{\Omega}_l)\big) \omega_l(\mathbf{x}) \boldsymbol{\phi}(\mathbf{x}) d\mathbf{x}, \quad (18)$$

where $\boldsymbol{\Phi}(\mathbf{x}) = (\Phi_1(\mathbf{x}), \cdots, \Phi_I(\mathbf{x}))^T$ and $\boldsymbol{\phi}(\mathbf{x}) = (\phi_1(\mathbf{x}), \cdots, \phi_J(\mathbf{x}))^T$[3]

Using these partial derivatives, $\{K_i^{(t-1)}\}_{i=1}^{I}$ and $\{\kappa_j^{(t-1)}\}_{j=1}^{J}$ can be updated using gradient-based local minimization techniques such as steepest descent and conjugate gradient.

To derive the update rule for $\{\widetilde{L}_l\}_{l=1}^{L}$, we must account for the constraint given by (7). Here, we minimize the Lagrange function

$$J(\boldsymbol{\Omega}, \boldsymbol{m}, \lambda) = E^{+}(\boldsymbol{\Omega}, \boldsymbol{m}) - \lambda\Big(\sum_{l=1}^{L} \widetilde{L}_l - 1\Big), \quad (19)$$

where $\lambda$ is a Lagrange multiplier.

The partial derivatives of $J(\boldsymbol{\Omega}, \boldsymbol{m}, \lambda)$ with respect to $\widetilde{L}_l$ and $\lambda$ are

$$\frac{\partial J}{\partial \widetilde{L}_l} = \frac{1}{\widetilde{L}_l} \iint_S (-\mathcal{D}_l(\mathbf{x}) + \mathcal{I}_l(\mathbf{x}; \boldsymbol{\Omega}_l)) d\mathbf{x} - \lambda \quad (l = 1, \cdots, L), \quad (20)$$

$$\frac{\partial J}{\partial \lambda} = -\sum_{l=1}^{L} \widetilde{L}_l + 1. \quad (21)$$

[3]In this paper, the partial derivatives of $E^{+}(\cdot)$ with respect to column vectors $\boldsymbol{K} = (K_1, \cdots, K_I)^T$ and $\boldsymbol{\kappa} = (\kappa_1, \cdots, \kappa_J)^T$ are defined as column vectors $\frac{\partial E^{+}}{\partial \boldsymbol{K}} = (\frac{\partial E^{+}}{\partial K_1}, \cdots, \frac{\partial E^{+}}{\partial K_I})^T$ and $\frac{\partial E^{+}}{\partial \boldsymbol{\kappa}} = (\frac{\partial E^{+}}{\partial \kappa_1}, \cdots, \frac{\partial E^{+}}{\partial \kappa_J})^T$, respectively.

Setting Equations (20) and (21) to zero, we obtain

$$\widetilde{L}_l = -\frac{q_l^{(t+1)}}{\lambda - p_l^{(t+1)}} \quad (l = 1, \cdots, L), \quad (22)$$

$$-\sum_{l=1}^{L} \widetilde{L}_l + 1 = 0, \quad (23)$$

where

$$p_l^{(t)} = \iint_S K_s^{(t)}(\mathbf{x})\, e^{-\kappa^{(t)}(\mathbf{x})\, \omega_l(\mathbf{x})} d\mathbf{x} \quad (l = 1, \cdots, L), \quad (24)$$

$$q_l^{(t)} = \iint_S \mathcal{D}_l^{(t)}(\mathbf{x}) d\mathbf{x} \quad (l = 1, \cdots, L), \quad (25)$$

where $K_s^{(t)}(\mathbf{x}) = \exp\big(\sum_{i=1}^{I} K_i^{(t)} \Phi_i(\mathbf{x})\big)$, $\kappa^{(t)}(\mathbf{x}) = \sum_{j=1}^{J} \kappa_j^{(t)} \phi_j(\mathbf{x})$, and $\mathcal{D}_l^{(t)}(\mathbf{x}) = m_l^{(t)}(\mathbf{x})\, D(\mathbf{x})$.

To update $\widetilde{L}_l^{(t)}$, we solve $L+1$ simultaneous equations (22) and (23) with $L+1$ unknowns $\{\{\widetilde{L}_l\}_{l=1}^{L}, \lambda\}$. By substituting Equations (22) into Equations (23), we get a fractional equation with an unknown variable $\lambda$

$$g^{(t+1)}(\lambda) \triangleq \sum_{l=1}^{L} \frac{q_l^{(t+1)}}{\lambda - p_l^{(t+1)}} + 1 = 0. \quad (26)$$

Hence, we numerically solve this equation using the Newton-Raphson method which iterates the following procedure until convergence:

$$\begin{aligned} \lambda^{(\tau_\lambda+1)} &= \lambda^{(\tau_\lambda)} - \frac{g^{(t+1)}(\lambda^{(\tau_\lambda)})}{g^{(t+1)\prime}(\lambda^{(\tau_\lambda)})} \\ &= \lambda^{(\tau_\lambda)} + \frac{1 + \sum_{l=1}^{L} \frac{q_l^{(t+1)}}{\lambda^{(\tau_\lambda)} - p_l^{(t+1)}}}{\sum_{l=1}^{L} \frac{q_l^{(t+1)}}{(\lambda^{(\tau_\lambda)} - p_l^{(t)})^2}}. \end{aligned} \quad (27)$$

Finally, by substituting those values into each of Equation (22), $\{\widetilde{L}_l\}_{l=1}^{L}$ can be updated.

## 5. Experimental Results

We evaluated the effectiveness of the proposed method on a synthetic scene and a real scene.

### 5.1. Synthetic Scene

We first evaluate the accuracy of the method using a synthetic image of a specular object. The simulated setup allows us to quantitatively evaluate the accuracy of the specular reflectance parameter estimates and illumination estimates. We rendered an image of a 3D model (Figure 3(b)) with spatially varying specular reflectance whose parameter values are shown in Figure 4. The illumination consisted of five point light sources. This synthetic image (Figure 3(a))

was then used as the input to the proposed algorithm. We located RBF centers $\boldsymbol{C}_i$ and $\boldsymbol{c}_j$ at regular intervals within the input image and fixed the values of RBF widths $R_i$ and $r_j$ at the interval between RBF centers ( $\{\boldsymbol{C}_i, R_i\}_{i=1}^{I}$ and $\{\boldsymbol{c}_j, r_j\}_{j=1}^{J}$ were equally set), as illustrated in Figure 3(c). The center and radius of each circle in Figure 3(c) indicate $\boldsymbol{C}_i$ ($\boldsymbol{c}_j$) and one quarter $R_i$ ($r_j$), respectively. From the input image, we detected a set of locally brightest points and used the viewing direction reflected about the surface normals at those surface points as the point source directions. Figure 5(a) shows the estimated $K_s(\mathbf{x})$ and Figure 5(b) shows the estimated $\kappa(\mathbf{x})$ encoded in RGB. The RMS errors of the estimated $K_s(\mathbf{x})$ and $\kappa(\mathbf{x})$ were 0.09 and 0.06, respectively.

Figure 6 show the result of rendering the object under a novel lighting condition (relighting). Figure 6(a) and Figure 6(b) show the synthesized images using the ground truth and estimated values of $K_s(\mathbf{x})$, $\kappa(\mathbf{x})$ and $\{\widetilde{L}_l\}_{l=1}^{L}$, respectively. Specular images were rendered using the estimated parameter values with the spherical Torrance-Sparrow reflection model which were then composed together with the relit diffuse images. The diffuse images were relit by simply taking the ratio of the incident irradiance between the original and new illumination environment, assuming Lambertian reflection.

The ground truth and estimated point source intensities are tabulated in Table 1. The results clearly show that the proposed method successfully estimates the illumination and spatially varying specular reflectance properties from a single specular reflection image with high accuracy.

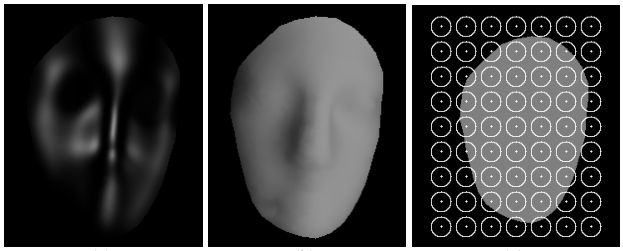

(a) (b) (c)

Figure 3. (a) A synthetic specular image. (b) The surface geometry used to render the synthetic specular image. (c) $\{\boldsymbol{C}_i, R_i\}_{i=1}^{I}$ ( $\{\boldsymbol{c}_j, r_j\}_{j=1}^{J}$ ).

Table 1. Estimated light source intensities.

| | Light 1 | Light 2 | Light 3 | Light 4 | Light 5 |
|---|---|---|---|---|---|
| Estimated light intensity | 0.1084 | 0.2010 | 0.2010 | 0.2410 | 0.1971 |
| Ground truth | 0.10 | 0.20 | 0.25 | 0.25 | 0.20 |

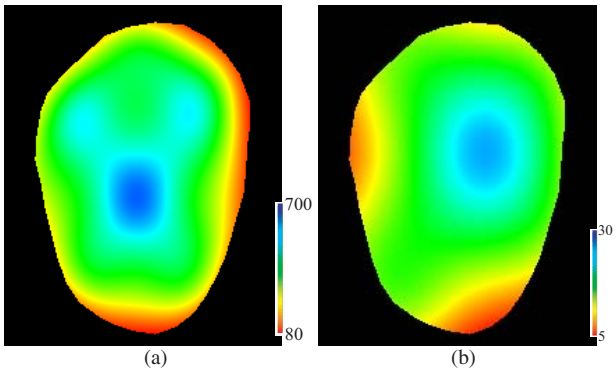


(a) (b)

Figure 4. Ground truth values of the spatially varying specular reflectance properties: (a) $K_s(\mathbf{x})$ and (b) $\kappa(\mathbf{x})$.

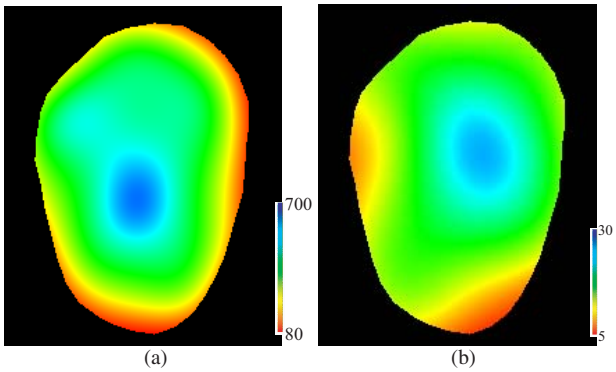


(a) (b)

Figure 5. Estimated spatially varying specular reflectance properties: (a) $K_s(\mathbf{x})$ and (b) $\kappa(\mathbf{x})$.

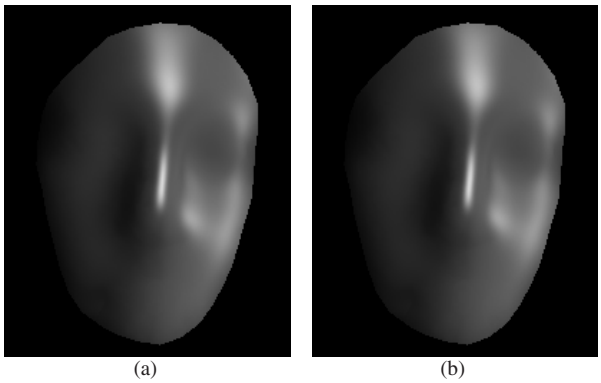

(a) (b)

Figure 6. Synthesized image under a novel lighting condition.

## 5.2. Real Scene

We also evaluated the effectiveness of the proposed method on a real scene. We set up a scene consisting of an assortment of fruits and vegetables: a watermelon, an orange pepper, a mango and a squash. For the illumination, we used 3 point light sources. We used a digital SLR (Canon 30D) to capture the image. In order to obtain a

specular-only image, we used a polarization filter [12, 18] in front of the light sources and camera lens, whose orientations were manually set to be perpendicular to each other to capture a diffuse-only image and then captured another image where the polarization filters were set to be parallel. Figure 7(a) shows the image taken with parallel polarization (diffuse+specular), Figure 7(b) shows the diffuse-only image, and Figure 7(c) shows the specular-only image computed by subtracting the diffuse-only image from the other input image. We also obtained a 3D geometric model for the objects using a laser range finder (Minolta Vivid 910) whose external orientation was pre-calibrated with the digital SLR. As in the previous example, from the specular image, we detected a set of locally brightest points and used them to estimate the point source directions.

Figure 8(a) shows the estimated values of $K_s(\mathbf{x})$ and Figure 8(b) shows the estimated values of $\kappa(\mathbf{x})$ encoded in RGB. One can see that the proposed method estimates the spatial variation of the specular reflection properties. For instance, $K_s(\mathbf{x})$ of the mango and $\kappa(\mathbf{x})$ of the squash are relatively large compared to the other three objects, and even within each object the values smoothly vary. Such information can be useful to classify the objects based on material properties. Note that, as shown in Figure 8, we cannot estimate the specular reflection properties where specular reflection is not observed. If necessary, we may directly extrapolate the estimated values using the radial basis functions or by assuming uniformity across local regions.

Figure 9 shows a rendered specular image using the estimated values of $K_s(\mathbf{x})$, $\kappa(\mathbf{x})$ and $\{\widetilde{L}_l\}_{l=1}^{L}$. The estimated and ground truth point source intensities are tabulated in Table 2. We measured the ground truth intensities by capturing an image of a black shiny sphere placed in the scene. The synthesized specular image clearly shows that the proposed method successfully estimates the illumination and spatially varying specular reflectance properties accurately. Note that the errors at the object boundaries, e.g., between the orange pepper and watermelon, are mainly caused by inaccuracy in the scanned geometry.

Figure 10 shows the results of rendering the scene under novel lighting conditions (relighting). In Figure 10(a) we turned off two light sources in the original illumination environment, and in Figure 10(b) we moved that light source to the left. The results clearly show that we can achieve photorealistic relighting of the scene with the estimated illumination and specular reflectance properties, which again strongly suggests that the proposed method accurately estimates these variables from a single specular image.

Table 2. Estimated light source intensities.

| | Light 1 | Light 2 | Light 3 |
|---|---|---|---|
| Estimated light intensity | 0.2826 | 0.3357 | 0.3817 |
| Ground truth | 0.2937 | 0.3371 | 0.3692 |

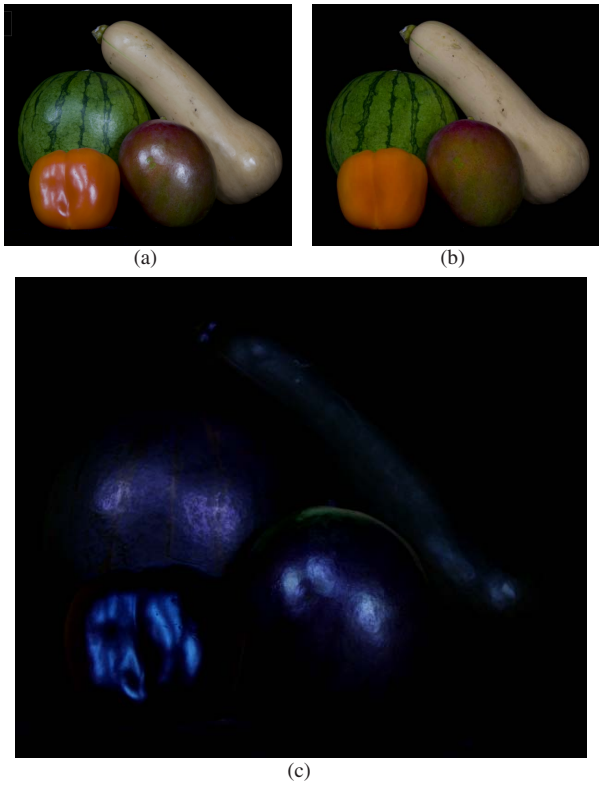

Figure 7. (a) One of the input images where both the diffuse and specular reflections are observed and (b) the other input image taken with orthogonal polarization filters to observe diffuse reflection only. (c) The specular image computed by subtracting (b) from (a) which is input to the proposed algorithm.

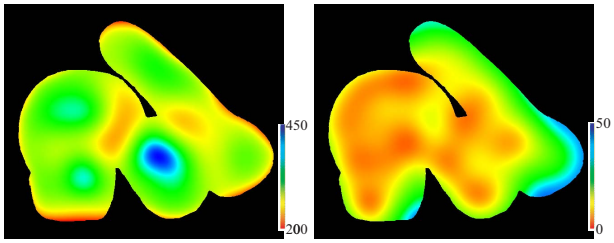


Figure 8. Estimated spatially varying specular reflectance properties: (a) $K_s(\mathbf{x})$ and (b) $\kappa(\mathbf{x})$.

## 6. Conclusion

We introduced a novel method for simultaneously estimating the illumination and spatially varying specular reflectance properties of an object, given a few images taken from the same viewpoint, e.g., in our setup two images, of an object of known geometry. The proposed method encodes specular reflection with a directional distribution and the spatially variation of its parameter values with a set of radial basis functions. This enables the formulation of the

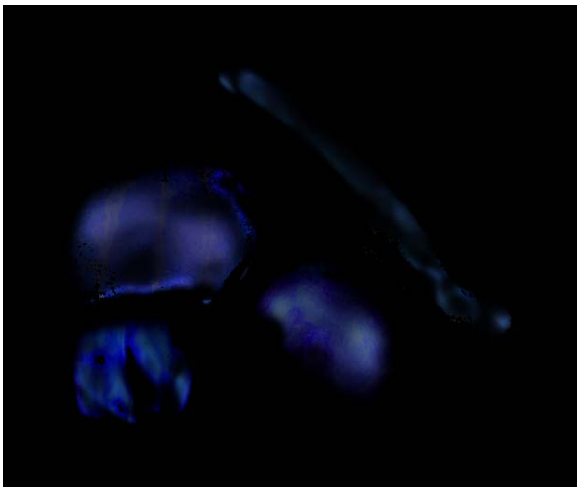

Figure 9. Synthesized specular image using the estimated $K_s(\mathbf{x})$, $\kappa(\mathbf{x})$ and $\{\widetilde{L}_l\}_{l=1}^{L}$.

(a) (b)

Figure 10. Synthesized images of the scene under novel lighting conditions.

simultaneous estimation as a sound probabilistic inference based on the $I$-divergence measure, which can be solved with an expectation maximization-like algorithm. We have shown its effectiveness through experiments with synthetic and real images. As future work, we would like to investigate the use of multiple images taken under varying illumination or viewpoints to densely estimate the specular reflectance properties across the entire object surface.

## Acknowledgement

This work was supported in part by National Science Foundation CAREER Award IIS-0746717 and the Japanese Ministry of Education, Science, and Culture under Grant-in-Aid for Scientific Research 20500155.

## References

[1] I. Csiszár. Why least squares and maximum entropy? - an axiomatic approach to inverse problems. *Ann. Stat.*, 19(4):2033–2066, 1991. 2, 4

[2] P. Debevec, T. Hawkins, C. Tchou, H. Duiker, W. Sarokin, and M. Sagar. Acquiring the reflectance field of a human face. In *Proc. ACM SIGGRAPH 00*, pages 145–156, 2000. 1

[3] A. Dempster, N. Laird, and D. Rubin. Maximum likelihood from incomplete data via the em algorithm. *J. Roy. Stat. Soc. B*, 39:1–38, 1977. 2

[4] R. Fisher. Dispersion on a sphere. In *Proc. Roy. Soc. London Ser. A.*, pages 295–305, 1953. 2

[5] D. Goldman, B. Curless, A. Hertzmann, and S. Seitz. Shape and spatially-varying brdfs from photometric stereo. In *Proc. ICCV*, pages 341–348, 2005. 2

[6] K. Hara, K. Nishino, and K. Ikeuchi. Mixture of spherical distributions for single-view relighting. *IEEE Trans. Pattern Anal. Mach. Intell.*, 30(1):25–35, 2008. 1, 2

[7] H. Kameoka, T. Nishimoto, and S. Sagayama. A multipitch analyzer based on harmonic temporal structured clustering. *IEEE Trans. Audio, Speech & Language Process.*, 15(3):982–994, 2007. 4

[8] G. Kay and T. Caelli. Inverting an illumination model from range and intensity maps. *CVGIP: Image Understanding*, 59(2):183–201, 1994. 1

[9] H. Lensch, J. Kautz, M. Goesele, W. Heidrich, and H. Seidel. Image-based reconstruction of spatially varying materials. In *Proc. EGWR*, pages 104–115, 2001. 1

[10] K. Mardia and P. Jupp. *Directional Statistics*. John Wiley & Sons, 2000. 2

[11] S. Marschner and D. Greenberg. Inverse lighting for photography. In *Proc. Color Imaging Conf.*, pages 262–265, 1997. 1

[12] S. Nayar, X. Fang, and T. Boult. Removal of specularities using color and polarization. In *Proc. CVPR*, pages 583–590, 1993. 7

[13] K. Nishino, K. Ikeuchi, and Z. Zhang. Re-rendering from a sparse set of images. *Department of Computer Science, Drexel University*, DU-CS-05-12, 2005. 1, 2, 3

[14] R. Ramamoorthi and P. Hanrahan. A signal processing framework for inverse rendering. In *Proc. ACM SIGGRAPH '01*, pages 117–128, 2001. 1

[15] Y. Sato, M. Wheeler, and K. Ikeuchi. Object shape and reflectance modeling from observation. In *Proc. ACM SIGGRAPH 97*, pages 379–387, 1997. 1

[16] F. Solomon and K. Ikeuchi. Extracting the shape and roughness of specular lobe objects using four light photometric stereo. In *Proc. CVPR*, pages 466–471, 1992. 3

[17] K. Torrance and E. Sparrow. Theory for off-specular reflection from roughened surfaces. *J. Optical Soc. Am. A*, 57:1105–1114, 1967. 2, 3

[18] L. Wolff and T. Boult. Constraining object features using a polarization reflectance model. *IEEE Trans. Pattern Anal. Mach. Intell.*, 13(6):635–657, 1991. 7

[19] T. Zickler, R. Ramamoorthi, S. Enrique, and P. Belhumeur. Reflectance sharing: Predicting appearance from a sparse set of images of a known shape. *IEEE Trans. Pattern Anal. Mach. Intell.*, 28(8):1287–1302, 2006. 1, 3